Structural study of $Al_{78}Mn_{17.5}Pt_{4.5}$ and (re)constitution of the Al–Mn–Pt system in its vicinity

Rimon Tamari[1], Benjamin Grushko[2,3], Louisa Meshi[1]

[1] *Department of Materials Engineering, Ben Gurion University of the Negev, Beer Sheva, Israel*
[2] *MaTecK GmbH, 52428 Jülich, Germany*
[3] *Peter-Grünberg-Institut, Forschungszentrum Jülich, 52425 Jülich, Germany*

Abstract

The previously reported Al–Mn–Pt X-phase with an unidentified structure (B. Grushko, J. Alloys Comp. 792 (2019) 1223) was concluded to be ternary extension of the binary orthorhombic Al–Mn T-phase. The geometry of the T-phase region in the Al–Mn–Pt phase diagram was updated and compared to the equivalent regions in other Al–Mn–(TM) systems (TM = Cr, Fe, Co, Ni, Cu, Pd). The lattice parameters of the $Al_{78}Mn_{17.5}Pt_{4.5}$ T-phase, corresponding to the high-Pt limit of its compositional region, were found to be a = 14.720(4) Å, b = 12.628(2) Å, c = 12.545(3) Å. The space group at this ternary composition was proved to be non-centrosymmetric P$na2_1$, instead of Pnam - which describes the symmetry of the binary Al-Mn T-phase. At the $Al_{78}Mn_{17.5}Pt_{4.5}$ composition, the Pt atoms are not distributed randomly in the Mn/Al sublattices, but adopt two specific Wyckoff sites, therefore, this structure should be regarded as an ordered variant of the T-structure. A partial atomic model of the $Al_{78}Mn_{17.5}Pt_{4.5}$ T-phase containing 8 Pt, 24 Mn and 36 (out of 124 expected) Al atoms was derived using electron diffraction tomography data. The positions of the heavy atoms match those proposed for the non-centrosymmetric model of the T–phase, which was previously disputed. Nanometric precipitates of the R-phase with the plate-like shape were identified in the ternary T-phase grains.

Keywords: Al-Mn-Pt; Transition metal alloys and compounds; Phase diagrams; Crystal structure; Electron crystallography.

1. Introduction

In the recent publication on the Al–Mn–Pt alloy system, a ternary so-called X-phase exhibiting a complex powder XRD pattern was reported between the $Al_{79.9}Mn_{15}Pt_{5.1}$ and $Al_{71.8}Mn_{25.5}Pt_{2.7}$ compositions, but its structure was not specified [1].

A thorough electron diffraction investigation, reported in current paper, allowed association of this structure with the orthorhombic high-temperature Al–Mn T-phase [2-9][1]. Reports on the atomic structure and even the symmetry of the T-phase are ambiguous. At first, binary Al_3Mn phase`s unit cell was found to be orthorhombic with Pnam space group [2]. Later, this symmetry was disputed by Shi *et al* [5], but detailed comparison of compatibility of the two models (in the framework of centrosymmetric Pnam and non centrosymmetric P$na2_1$ space groups) to the single crystal X-ray diffraction data ruled out the non-centrosymmetric option [6]. T-phases, revealed in

[1] This designation is more reasonable than Al_3Mn or h-$Al_{11}Mn_4$ used in the literature due to its existence in a wide binary compositional region and wide extensions in many ternary alloy systems. See also additional arguments below.

ternary systems, such as Al-Mn-Pd [4], exhibited various atomic models. In general, ternary Al-TM1-TM2 (where TM1 and TM2 are transition metals) T-phase`s atomic models, changed as a function of the Al/TM1 ratio and the type and/or amount of the TM2 element [5-7]. Therefore, atomic model of the ternary Al-Mn-Pt T-phase required an independent solution of its atomic structure.

Partial atomic model of the $Al_{78}Mn_{17.5}Pt_{4.5}$ T-phase was successfully derived after determination of the space group as non-centrosymmetric P*na*2_1, contrarily to the P*nam* space group of the binary Al-Mn T-phase. Subsequently, the above-mentioned X-phase region was recognized as a ternary extension of the binary T-phase. The Al–Mn–Pt constitutional diagram was modified in the compositional region adjacent to Al_3Mn-Al_4Mn and compared to the equivalent regions in other Al–Mn–TM alloy systems (TM = Cr, Fe, Co, Ni, Cu, Pd).

2. Experimental

The experiments were carried out on an $Al_{78}Mn_{17.5}Pt_{4.5}$ alloy, studied previously in Ref. [1]. The purity of Al was 99.999 %, of Mn 99.99 %, of Pt 99.9 %. The sample was annealed at 800 °C under vacuum of $9x10^{-7}$ mBar for 622 h. The scanning electron microscopy (SEM, JEOL 840a equipped with EDAX Genesis 200 emission spectroscopy system) was carried out on polished unetched surfaces. Standard deviation of measurements was of the order ±0.5 at.%. The powder X-ray diffraction (XRD) examinations were carried out using Cu Kα1 radiation and an imaging plate (Huber G670). Other fragments were studied using a Rigaku D/MAX-2000 diffractometer equipped with a graphite monochromator for Cu Kα radiation. The measurements were performed within 2θ range from 5 to 100° at a 2θ step size of 0.02° with the counting rate of 10 s/step and the FULLPROF software [10] was used for an analysis of the XRD data.

For the Transmission Electron Microscopy (TEM) analysis, the alloy was ground into powder using an agate mortar and pestle, dispersed in isopropanol and stirred in the ultrasonic bath. This suspension was dropped on a carbon-coated Cu TEM grid. The electron diffraction tomography (EDT) data collection was performed manually in the selected area electron diffraction (SAED) mode. From a single particle, a series of the off-axis patterns was recorded at constant tilt step of 1° in the range of ±44°. Electron diffraction (ED) patterns were recorded on FEI T-12 Tecnai TEM (LaB_6 source) operating at 120 kV with the goniometer tilt range of ± 60. A series of electron diffraction frames were processed and merged using PETS 2.0 software [11]. Structure solution was performed using Direct Methods (DMs) incorporated in the SIR2011 package [12]. Least-squares refinement was performed using SHELXL97 [13].

Scanning TEM (STEM) and High Resolution TEM (HRTEM) investigations were carried out on a JEOL JEM-2100F TEM operating at 200 kV equipped with JED-2300T Energy Dispersive Spectrometer (EDS), scanning coils and GATAN 806 high-angle annular dark field (HAADF) detector.

3. Results and discussion

3.1. Correlation of the Al–Mn–Pt X-phase and the Al–Mn T-phase.

Previously, the Al–Mn–Pt phase diagram has been studied mainly at 1100 and 800°C and several additional Al-rich alloys have been examined at intermediate 1000 and 900 °C [1]. The ternary region, associated with the X-phase, has only been bordered in the 800 °C isothermal section. The powder XRD pattern of an $Al_{78}Mn_{17.5}Pt_{4.5}$ alloy, annealed at 800 °C and verified by

metallographic examinations to be essentially single-phase, indicated a complex structure (Fig.1a) which has not been specified earlier [1]. In fact, the lower-Pt limit of the above-mentioned X-phase region is quite close to the compositional region of the Al–Mn T-phase. However, the latter is stable in binary compositions at somewhat higher temperatures (see Fig.2a, Ref. [14] and references therein). Furthermore, the comparison of the diffraction profile in Fig.1a to that of an $Al_{75}Mn_{25}$ T-phase (Fig.1b) did not allow concluding their sufficient similarity. Unfortunately, at 900 °C, i.e. inside the temperature range of the binary T-phase stability, only the upper-Al limit of the X-phase was determined (see Fig.2b).

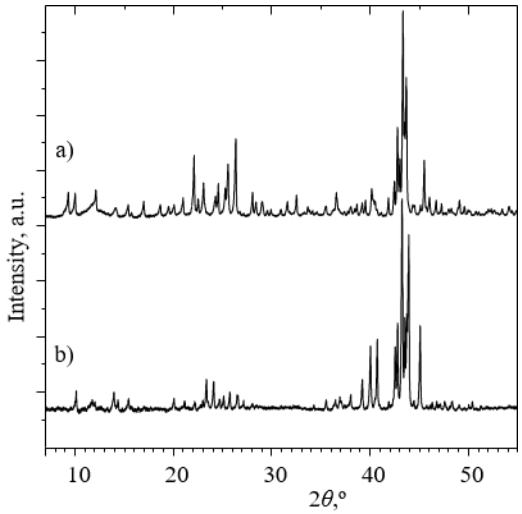

Fig. 1. XRD patterns taken from the: a) $Al_{78}Mn_{17.5}Pt_{4.5}$ alloy, annealed at 800 °C for 622 h; b) $Al_{75}Mn_{25}$ alloy, annealed at 900 °C for 68 h.

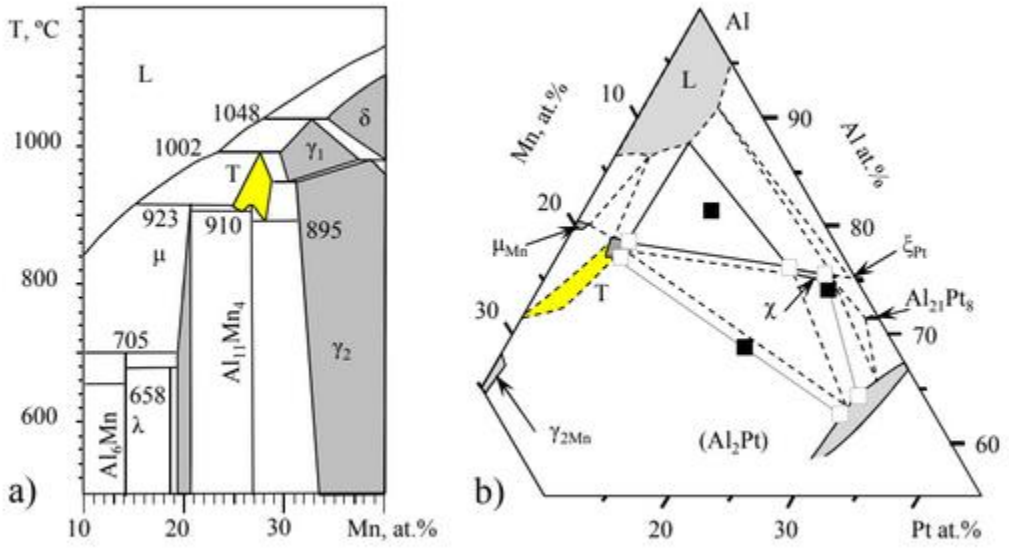

Fig. 2. a) Partial binary Al-Mn phase diagram [14]. b) The phase equilibria in the Al-rich part of Al-Mn-Pt at 900 °C, determined in Ref [1]. The region of the T-phase (marked by yellow) is shown extended from the binary compositions basing on the present results. (For the interpretation of the colors see the online version)

Therefore, electron diffraction (ED) examinations were suggested for the validation of the structure of the phase forming in the $Al_{78}Mn_{17.5}Pt_{4.5}$ alloy annealed at 800 °C. The ED patterns, shown in Figs.3a-c, confirmed its geometric similarity to the binary T-phase and the stabilization of the binary T-phase by Pt at lower temperatures.

The electron diffraction patterns of the T-phase, taken from several particles, exhibited some smearing of the diffraction reflections (see Fig.3d). The corresponding real-space images revealed a fine plate-like precipitation of an additional phase (Fig.3e). The precipitates were associated with the so-called R-phase (see below). Probably they are formed during cooling from the annealing temperature.

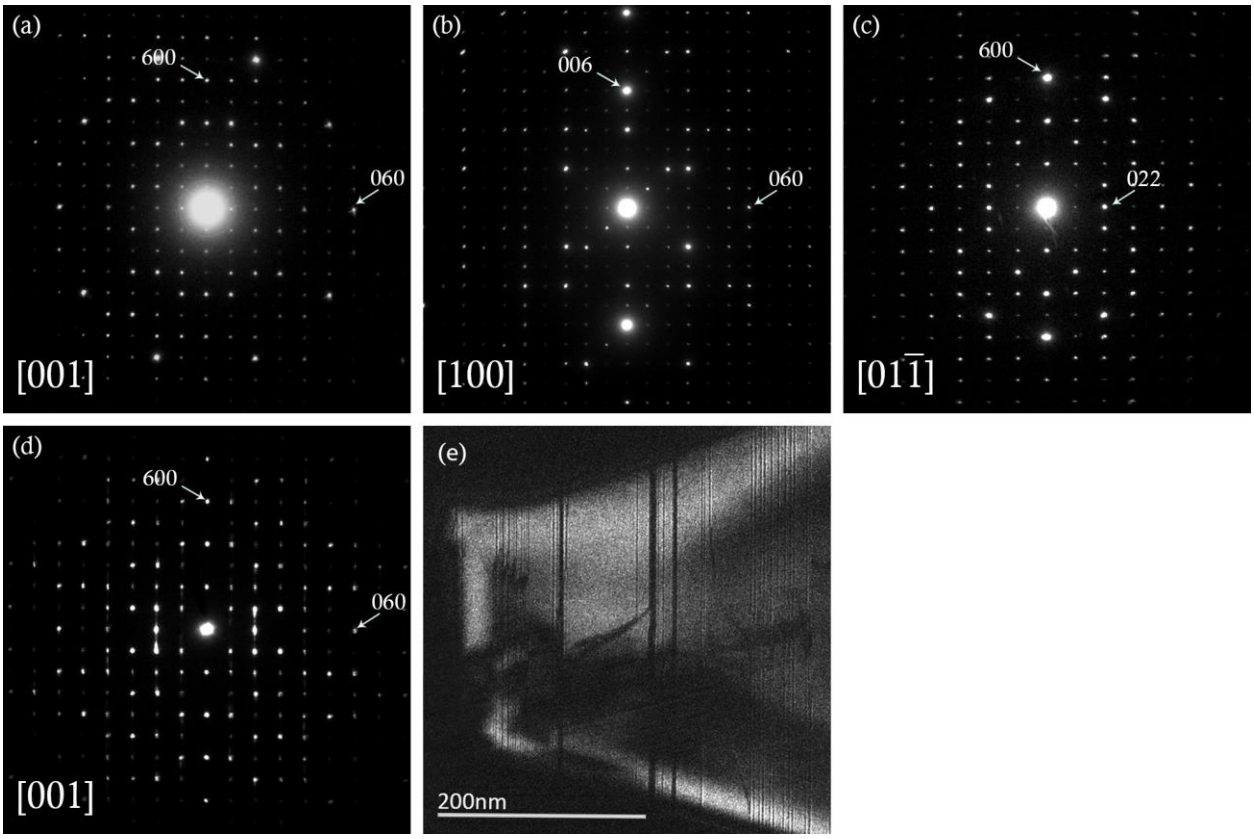

Fig. 3. SAED patterns of the T-phase taken at (a) [001], (b) [100], (c) [01$\bar{1}$] zone axes. In (d) some smearing of the reflections in the [001] pattern of the T-phase is visible. The dark field image taken from the same region at $g = (020)_T$ and illuminating the T-matrix (e) visualizes the plate-like precipitates with the interface parallel to $\{100\}_T$. Forbidden by symmetry reflections are seen at some ED patterns due to double-diffraction phenomenon.

The total fraction of the second phase seemed to be not significant. Subsequently, the composition of the T-phase was not much different from that of the total alloy composition. The

powder XRD pattern in Fig.1a could be indexed according to the space group P*na*2_1, or P*nam*, and the lattice parameters a = 14.720(4) Å, b = 12.628(2) Å and c = 12.545(3) Å (Average $\Delta(2\theta)$ = 0.009°, Maximum $\Delta(2\theta)$ = 0.061°, FOM F(30) = 52.8 for total 133 reflections). For comparison, the lattice parameters of the $Al_{75}Mn_{25}$ T-phase, corresponding to the powder XRD pattern in Fig.1b, are a = 14.890(2) Å, b = 12.441(3) Å and c = 12.564(3) Å (Average $\Delta(2\theta)$ = 0.009°, Maximum $\Delta(2\theta)$ = 0.046°, FOM F(30) = 20.9 for total 54 reflections). The powder XRD pattern of the binary $Al_{75}Mn_{25}$ T-phase and that calculated from the previously reported model [6] for the above-mentioned lattice parameters are in fair agreement. This is not a case for the powder XRD pattern of the $Al_{78}Mn_{17.5}Pt_{4.5}$ T-phase. This item will be discussed below.

3.2. Compositional regions of the T-phase in Al–Mn–Pt and other Al–Mn–TM systems.

Considering the present results, the updated overall compositions of the phases, revealed in the Al-rich part of the Al–Mn–Pt system at 800-1100 °C, are shown in Fig. 4. Accordingly, the composition of ~$Al_{79.5}Mn_{15.5}Pt_5$ corresponds to the maximal observed propagation of the T-phase region in the Al–Mn–Pt.

Since at 800 °C, the T-phase is already unstable at binary compositions, the former ternary region of the X-phase in the partial 800 °C isothermal section (presented in [1]) could be simply renamed, and no corrections are required for the 1100 and 1000 °C sections[1]. Only the partial 900 °C isothermal section of Ref. [1] is slightly modified in the present paper, see Fig.2b, namely the ternary region of the former X-phase is connected to that of the binary T-phase.

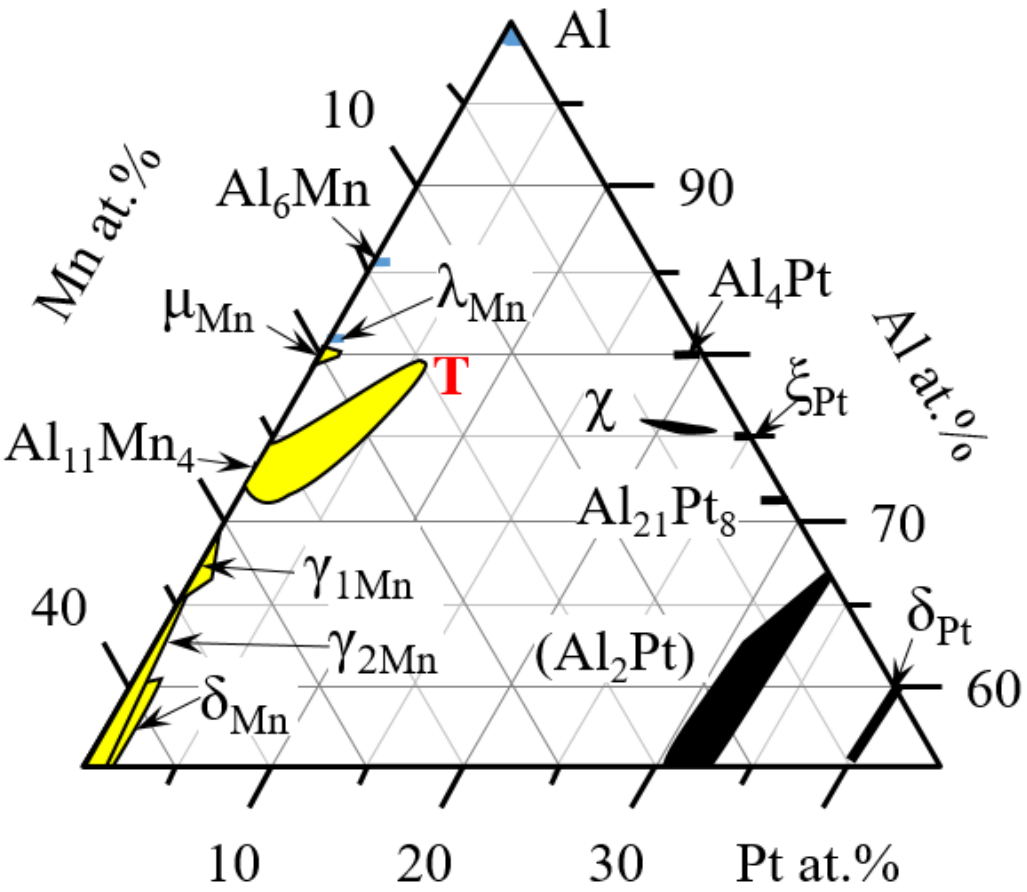

Fig. 4. Overall compositions of the phases in the Al-rich region of Al–Mn–Pt at 800 -1100 °C. (For the interpretation of the colors see the online version)

The noticeable ternary extension of the compositional region of the T-phase towards higher Al content is in contrast to that of numerous binaries in the known ternary phase diagrams of Al with transition metals (TMs) of the VI-VIII groups, where the atoms of one TM are replaced by the atoms of the other TM and not by Al (see [15], for example). Thus, in the alloy systems with both TMs from the same column of the Periodic Table, the phases are usually extended along about a constant Al concentration. The dissolution of a later TM in an Al-rich compound with an earlier TM - results in a slight decrease of its Al concentration; while the dissolution of Cu or Zn - sharply decreases the Al concentration. This behavior implies approximately constant electron-to-atom ratios along the whole compositional regions. In these Al-rich phases both TMs exhibit negative valences because of the absorption of electrons supplied by trivalent Al for filling their d-orbitals, and, since, saturation of the orbitals in the later TMs requires less Al than for the earlier TMs. In the Al–Cu(Zn)–TM alloy systems, positive-valent Cu (or Zn) replaces positive-valent Al in the Al–TM phases.

As to the ternary extensions of the Al–Mn T-phase (see Fig. 5 [15, 16-22]), apart from the *increased* Al concentration with the dissolution of Pt or Pd, the dissolution of Cu also does not reduce the Al concentration of the T-phase as sharp as, for example, the Al concentration of the $Al_{13}TM_4$ phases (TM = Fe, Co, Ru, see [15a]). In the Al–Mn–Co(Ni) alloy systems, the “would

be" propagation of the T-phase towards higher Al is visibly suppressed in favor of the φ-phase[2], while in the Al–Mn–Fe system the φ-phase and T-phase mutually limit their compositional regions (see [15b] and references therein). In order to come to an agreement between these observations and the above-mentioned general rules for the Al-rich phases` formation in the Al–TM1-TM2 systems, one could suggest the possibly *higher*-Al stoichiometry of the binary T-phase than any of its equilibrium compositions in the phase diagram in Fig. 2a.

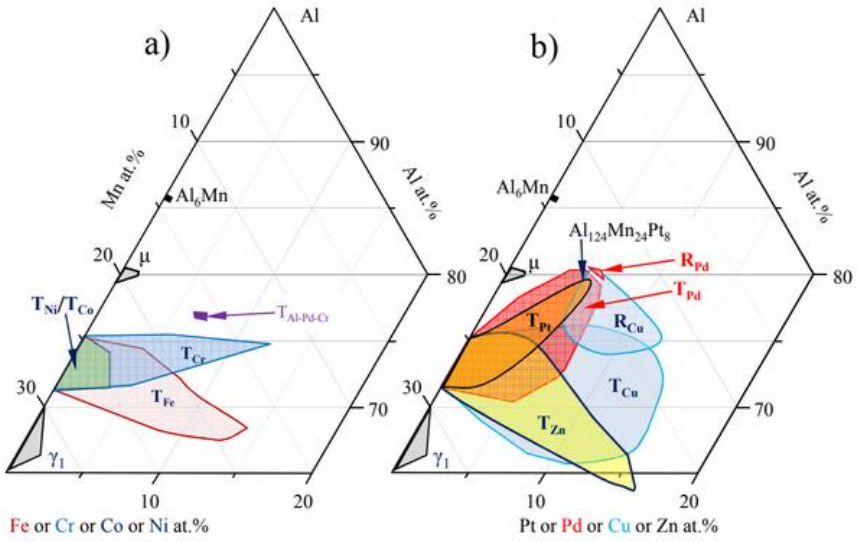

Fig. 5. Overall compositions of the ternary extensions of the T-phase in the Al–Mn–TM alloy systems (where TM = Cr [21], Fe [20], Co [15b], Ni [19], Cu [17], Zn [unpublished work], Pd [16], Pt (present work)), in Al–Cr–Pd [22] and the overall compositional regions of the R-phases in Al–Mn–Pd [16] and Al–Mn–Cu [17]. (For the interpretation of the colors see the online version)

According to the structural models, generally accepted for the T-phase ([4-9], for example) there are 156 atoms in the unit cell, occupying 4-fold and 8-fold sites. Many of these positions are reported to have partial occupancy, i.e. both Al and Mn occupy the same sites. If the positions, where Mn/Al ≤ 1, would be completely occupied by Al and others, where Mn/Al > 1, by Mn - an ideal stoichiometry of $Al_{124}Mn_{32}$ (i.e. ~$Al_{79.5}Mn_{20.5}$) would be achieved. This composition is *outside* the stability region of the T-phase, but one can suggest its virtual formation above the equilibrium melting temperatures and actual formation under non-equilibrium conditions. In fact, a structure, isotypical to the T-phase, has been observed by electron diffraction in a rapidly solidified Al_4Mn alloy together with the decagonal quasicrystals [23]. Unfortunately, no compositional measurements of these phases were reported.

The replacement of some Mn or Al by Pt or Pd in suggested $Al_{124}Mn_{32}$ could stabilize the T-phase. For example, if one 8-fold or two 4-fold positions of Mn/Al are completely replaced by Pt, the resulting composition would be $Al_{124}Mn_{24}Pt_8$, i.e. close indeed to $Al_{79.5}Mn_{15.5}Pt_5$ mentioned above as the lower-Mn limit of the T-phase region. Such full occupancy of specific sites is an ordering phenomenon which, in turn, might change the symmetry of the structure. Thus, the incorporation of Pt in the structure of the T-phase requires a structure solution.

[2] The $Al_{10}Mn_3$ φ-phase of the Al_5Co_2–type structure is metastable in Al–Mn and is stabilized by some addition of Fe, Co or Ni.

3.3. Crystal structure of the ternary Al–Mn–Pt T-phase.

A further structural study of the T-phase was performed on the above-mentioned $Al_{78}Mn_{17.5}Pt_{4.5}$ alloy, annealed at 800 °C. The FULLPROF software [10] was used in the profile matching mode (i.e. refining only the geometry, without taking into account the atom positions). As a result, the R_p = 4.76 %, R_{wp} = 6.55 % and R_B = 0.68 % reliability factors were attained. The calculated and observed X-ray diffraction profiles and the difference between them, as obtained following the profile matching routine, are shown in Fig. 6.

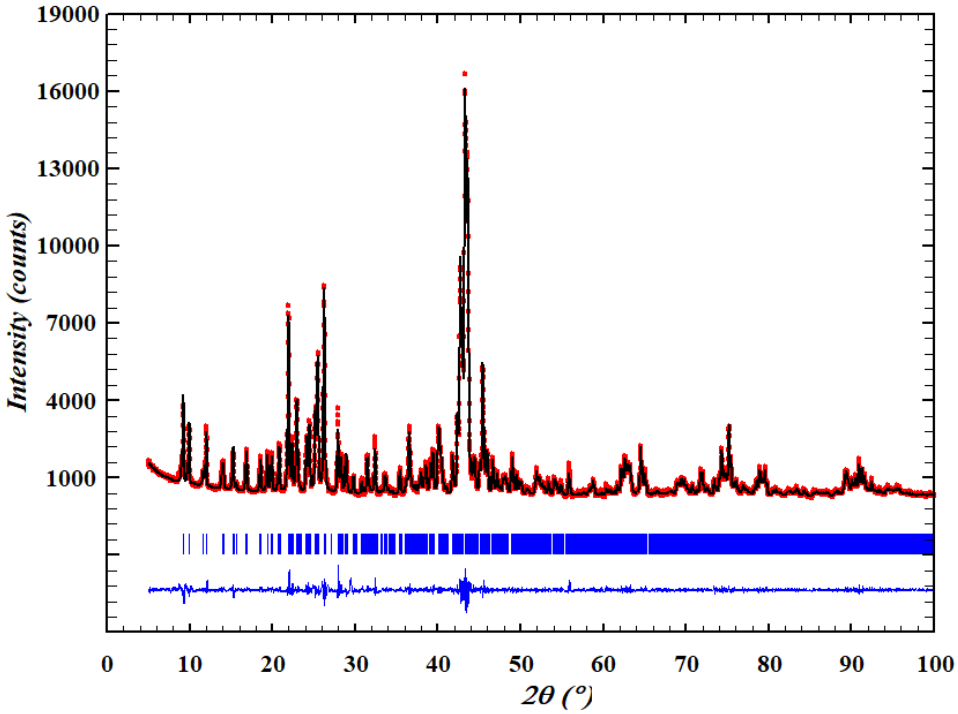

Fig. 6. Plot of the refinement of the $Al_{78}Mn_{17.5}Pt_{4.5}$ T-phase structure showing: observed X-ray profile (filled circles), calculated profile (solid line) and difference between them (on the bottom). Vertical bars refer to the calculated peak positions of the T-phase (For the interpretation of the colors see the online version).

An attempt to perform the Rietveld refinement of the above-mentioned powder XRD pattern using the atomic models proposed in the framework of the P*nam* space group (binary or ternary)[4], [6] or previously reported model with non-centrosymmetric P*na*2_1 symmetry [5] led to strong divergence. Furthermore, an effort to use the structure factors extracted from the XRD data, shown in Fig. 6, for full structure solution was also unsuccessful. Therefore, a structure solution of the ternary T-phase was performed using electron diffraction tomography (EDT) method. A series of the ED frames, collected from a single particle of the T-phase (essentially free from the above-mentioned precipitates), was processed. The corresponding projections of the reconstructed reciprocal lattice along the highest symmetry axes are presented in Figs. 7a-c. Resemblance between Figs. 7a,c and Figs. 3a,b is evident. The cylindrical projection, shown in Fig. 7e, presents sharp peaks, indicating good reconstruction of the 3D reciprocal lattice and, thus, a satisfactory data for the structure solution. The reciprocal space is not complete due to the

"missing cone" problem [24] (i.e. limited tilt of the goniometer in the microscope, its magnitude is presented in Fig.7d).

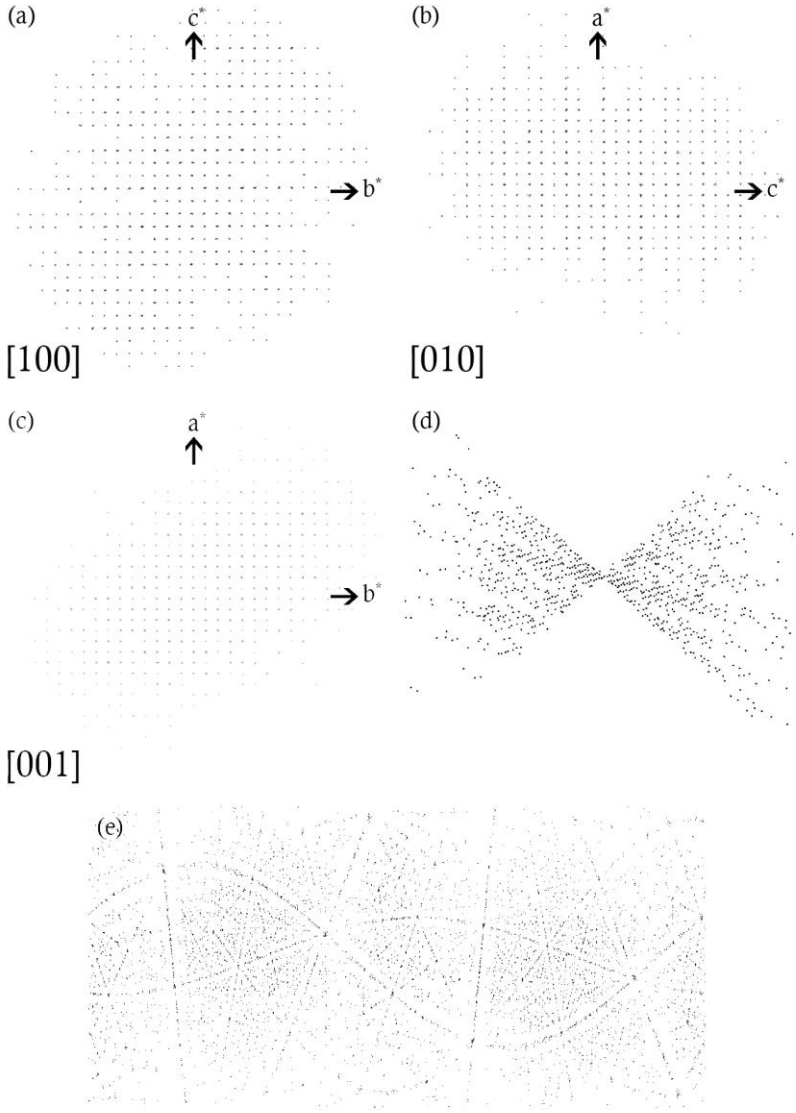

Fig. 7. 3D reconstruction of the reciprocal space. EDT data were taken from a single particle of the T-phase. (a-c) Projections along the [100], [010] and [001] orientations, respectively. (d) Representation of the "missing cone" magnitude. (e) Cylindrical projection of the reconstructed reciprocal space.

Since both P*nam* and P*na*2_1 space groups were suggested in the literature for the T-phase, both symmetries were applied for structure solution performed using direct methods, incorporated in the SIR2011 software [12]. The retrieved reliability factors were: R_1= 31.1% (for the P*na*2_1 space group) and R_1= 37.3% (for the P*nam* space group). The assignment of the atomic positions of the heaviest Pt atoms was evident since in both models the height of peaks, attributed to the Pt atoms, was twice higher than those assigned to Mn. The amount of the proposed Pt atoms was different – 8 for the P*na*2_1 case and 4 for the P*nam* one (see below).

Although in the literature both P*nam* and P*na*2_1 space groups were suggested as candidates to describe the symmetry of the binary T-phase [4, 5], there is a clear preference to the former following a thorough crystallographic analysis made in [6]. Moreover, an atomic model of the ternary $Al_{72.3}Mn_{24.5}Pd_{3.2}$ T-phase [9] was also solved in terms of centrosymmetric P*nam*. However, in our case, the structure solution for $Al_{78}Mn_{17.5}Pt_{4.5}$ provided better reliability factors for the non-centrosymmetric space group. Furthermore, the unit cell of the $Al_{78}Mn_{17.5}Pt_{4.5}$ T-phase should contain 8 Pt atoms (according to the chemical composition measured by EDS), which imposes their occupancy of either one 8-fold or two 4-fold positions (not taking partial occupancy into an account). The solution in the framework of the centrosymmetric space group (P*nam*) places Pt only at one 4*c* position. The other 4*c* positions had much lower heights at the potential map, hinting their occupancy by Mn and/or Al atoms. This is not enough for the measured composition and does not allow a reasonable interpretation of the high-resolution high-angle annular dark filed (HAADF) images obtained from the T–phase. The HAADF images provide a possibility to observe the projection of the atomic columns at atomic resolution with a contrast depending on the atomic number. Thus, the columns containing the Pt atoms, which are the heaviest scatterers in this unit cell, produce the brightest spots. The HAADF images taken along the principle perpendicular orientations [100] and [001] are shown in Fig. 8. In Fig. 8a, the eight bright spots per the unit cell projection correspond to the columns of the Pt atoms.

In general, the atomic models with the P*nam* symmetry, proposed in [6, 9], do not contain additional (to proposed) positions for the Pt atoms which would be consistent with the HAADF images, while the proposed two 4-fold positions of the Pt atoms in the framework of P*na*2_1 fitted these images reasonably well, see Fig. 8. Therefore, it was concluded that the space group which describes the symmetry of the unit cell of the $Al_{78}Mn_{17.5}Pt_{4.5}$ T-phase is P*na*2_1.

The atomic model, corresponding to the P*na*2_1 case underwent kinematical least-squares refinement ($I \propto |F|^2$) vs. EDT data using SHELXL97 [13]. After each refinement cycle the stability of the model (shift of atom positions and thermal motion parameters) was checked. Although not all Al atoms were found in the last cycle, the refinement procedure was stopped since the Fourier map was flat and stability was reached. The refinement resulted in not significant shifts of the atom positions and reasonable thermal motion parameters (see Table 1). The partial model contained all heavy atoms (8 Pt and 24 Mn) and 36 out of the 124 expected Al atoms.

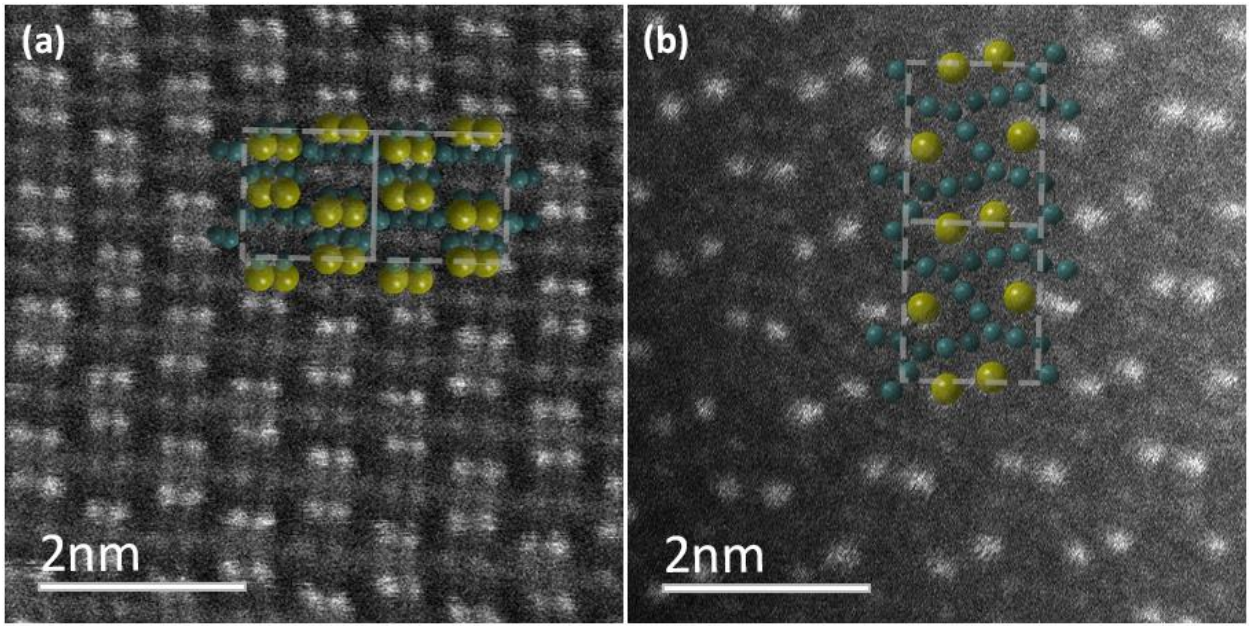

Fig. 8. HAADF images taken from the $Al_{78}Mn_{17.5}Pt_{4.5}$ T-phase along the: (a) [100] and (b) [001] orientations. For clarity, the proposed atomic model of the T-phase containing only the Pt (big light-green spheres) and Mn (small dark-green spheres) positions is overlaid on the image. A projection of two unit cells (marked by dashed line) is shown at each image. (For the interpretation of the colors see the online version.)

For validation, the partial atomic model developed here was overlaid on the HAADF images taken at principal orientations (Figs. 8a,b) Similarity is evident. Furthermore, the retrieved heavy atoms positions were compared to the model reported in [5], where the non-centrosymmetric P*na*2_1 space group was used. Table 2 shows the distances between the correlating atomic positions, as calculated using the COMPSTRU tool [25]. Small distances between the correlating positions (less than 0.9 Å) and measure of similarity (defined in [26]) of 0.084 mean that the models are very similar. On the other hand, this comparison also points to the differences between the binary [5] and ternary models. First, the Mn atoms occupy only a part of the Mn positions assigned to these atoms in the binary model, while some Mn atoms in the ternary model occupy the positions fully assigned to Al in the binary model. Second, the Pt atoms occupy one position assigned in the binary model to Mn and another assigned in binary to Al. These results point to an ordering and not to a simple substitution of Al and Mn atoms by Pt.

The reason for the difficulties in the modeling of the T-phase in the title alloy and probably also in the change of its space group could follow from the lattice distortions appearing at the higher-Al limit of its compositional region, and they are inevitable under the current experimental conditions. Indeed, the fact of the above-mentioned second phase precipitation, occurring rather by cooling than resulting from an annealing at 800 °C, indicates a strong super-saturation of the T-phase at room temperature in the precipitation-free regions. Its relaxation would be only possible by the phase separation under equilibrium conditions at somewhat lower annealing temperatures.

Table 1. Atomic coordinates and isotropic thermal parameters for the $Al_{78}Mn_{17.5}Pt_{4.5}$ T-phase.

Atom	Wyckoff site	x	y	z	U
Pt1	4a	0.9609(8)	0.6617(4)	0.0132(4)	0.2255(0)
Pt2	4a	0.9611(0)	0.6562(9)	0.3739(9)	0.1327(0)
Mn1	4a	0.6831(0)	0.6579(7)	0.5027(3)	0.0587(9)
Mn2	4a	0.7504(8)	0.5000(8)	0.8543(6)	0.0700(6)
Mn3	4a	0.7093(8)	0.8283(7)	0.8363(9)	0.0752(6)
Mn4	4a	0.9414(7)	0.0715(8)	0.6563(0)	0.0814(0)
Mn5	4a	0.7798(1)	0.3251(6)	0.6838(4)	0.0732(4)
Mn6	4a	0.5667(9)	0.5475(5)	0.8160(1)	0.0439(8)
Al1	4a	0.7470(9)	0.9962(7)	0.7042(3)	0.0791(8)
Al2	4a	0.7215(0)	0.8199(9)	0.6394(8)	0.0547(6)
Al3	4a	0.0595(6)	0.6457(9)	0.6211(5)	0.0352(9)
Al4	4a	0.6404(3)	0.3166(2)	0.5277(5)	0.0502(2)
Al5	4a	0.0575(9)	0.4518(0)	0.2393(1)	0.0260(4)
Al6	4a	0.8842(3)	0.6743(7)	0.5563(8)	0.0352(6)
Al7	4a	0.6418(9)	0.6695(0)	0.3080(5)	0.0222(0)
Al8	4a	0.6785(5)	0.6589(4)	0.7302(5)	0.0274(8)
Al9	4a	0.9358(0)	0.7590(1)	0.7488(5)	0.0178(4)

Table 2. Absolute distances between the positions of the heavy atoms in the $Al_{78}Mn_{17.5}Pt_{4.5}$ T-phase, as found in the present work, and the corresponding Mn/Al atoms in the model reported in Ref. [5].

Partial ternary $Al_{78}Mn_{17.5}Pt_{4.5}$ T-phase model [this work]	Binary T- phase model [5]	Distances between the corresponding atom positions, [Å]
Pt1	Al28	0.45
Pt2	Mn23	0.55
Mn1	Mn30	0.31
Mn2	Mn19	0.57
Mn3	Mn20	0.37
Mn4	Mn25	0.83
Mn5	Al4	0.31
Mn6	Al2	0.26

3.4. R-phase in Al–Mn–Pt system

Apart from the above-mentioned streaks in the ED patterns of the T-phase (see Fig. 3d), no additional effect which could help in the identification of the precipitates, forming inside the T-phase matrix, was observed. However, some information concerning the structure of the precipitates can be obtained by examination of the corresponding high resolution TEM (HRTEM)

images. Fig. 9a shows such an image in the same orientation as the ED patterns, presented in Figs. 3d,e. Fourier transform of the T-matrix (Fig. 9b) exhibits a rectangular reciprocal unit cell with the ratio of edges ~ 1.17 matching to that of $(a/b)_T = 1.166$. Fourier transform, taken from a precipitate (Fig. 9c), also exhibits a rectangular reciprocal unit cell with a centering and the ratio of edges ~ 3.1. Using the lattice parameters of the T-phase as a standard, the d-spacing of the marked nodes of the precipitate's lattice can be estimated as 7.7 Å and 24 Å. These values are close to the lattice parameters *a* and *b* of the so-called R-phase, which coexists with the ternary extension of the T-phase in the Al–Mn–Pd alloy system at comparable equivalent compositions [3, 9, 16].

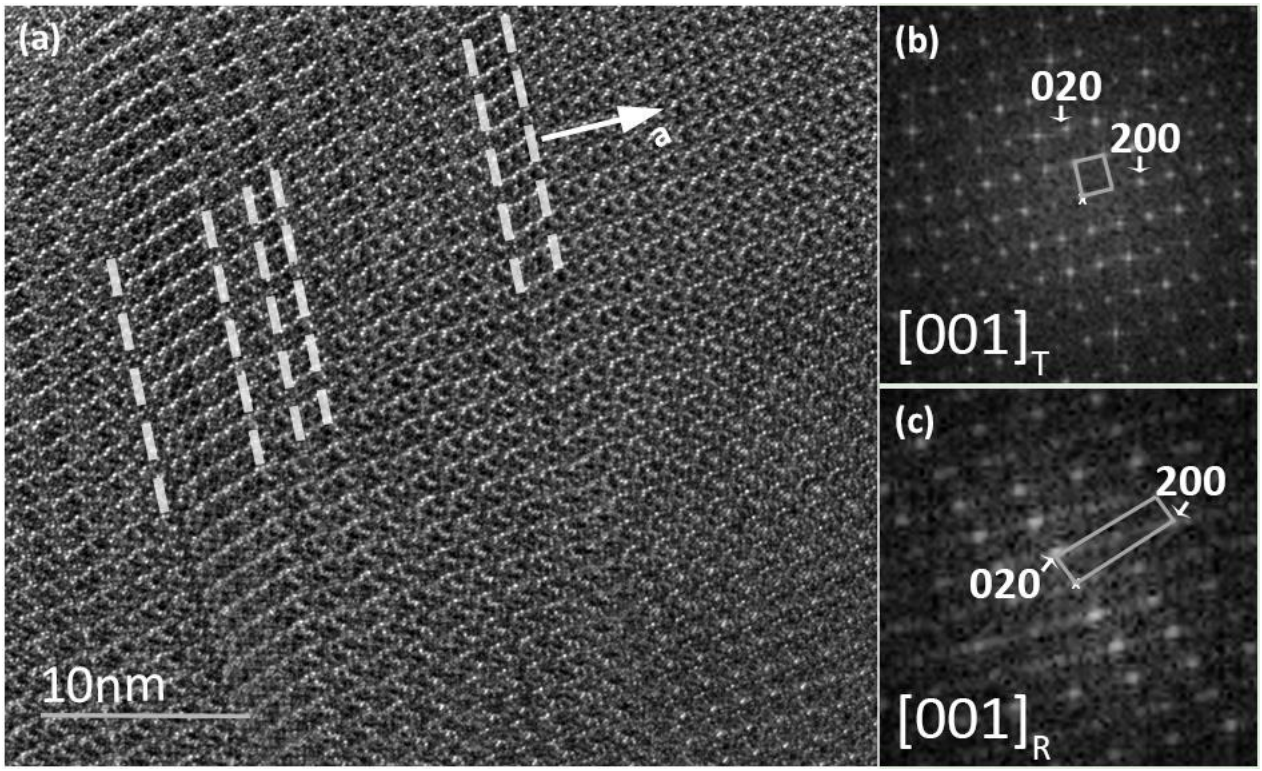

Fig. 9. (a) HRTEM image showing the interfaces, where the T-phase is the matrix and the inclusions are the R-phase (parallel boundaries are marked by dashed lines). (b) Fourier transform taken from the region of the T-phase. (c) Fourier transform taken from the region of the R-phase. Small "x" marks a center of the transform. For visualization of the rectangular unit cell in reciprocal space - rectangles were marked on Fourier transforms.

The Al-Mn-Pd R-phase was found to be orthorhombic (C*mcm*, a = 7.76 Å, b = 23.88 Å and c = 12.43 Å) [3], where it was originally proposed in the B*bmm* setting]. The Al-Mn-Pd T- and R-phases have very close lattice parameters c and the volumes of their unit cells, while $b_R/a_T \approx b_T/a_R$ and this ratio is close to the golden mean $\tau = (\sqrt{5}+1)/2$. Although the c lattice parameter of the above–mentioned precipitates could not be verified under the conditions of our experiment, its association with the R-phase is very plausible considering the above-mentioned items and its similar formation in Al-Mn-Pd. Consequently, the pattern in Fig. 9c can be indexed and the orientation relationship between the T-phase and suggested R-phase can be defined as: $[001]_T||[001]_R$; $(100)_T||(1\bar{1}0)_R$, i.e. the same as in Al-Mn-Pd [3]. Combining the information obtained from the TEM images and the corresponding ED patterns, the plane of the interface was

concluded to be $\{100\}_T$, see Figs. 3d,e and Fig. 9. As follows from the analysis of their structures, the R- and T-phases are constructed from the same building elements arranged parallel in R and in a herringbone manner in T [3]). This is also demonstrated by the HRTEM images of the projections perpendicular to the *c*-axis, Fig. 9a. The herringbone-like arrangement of bright spots is clearly visible in the HAADF image (taken at the same [001] orientation of the T-phase) and the overlaid atomic model in Fig. 8b.

In the Al–Mn–Pd system, the R-phase was found at 700 °C slightly outside the compositional range of the T-phase (see Fig. 5b). Some overlap of the R-T compositional regions at lower temperatures is not excluded, see for example Al–Mn–Cu system (see Fig. 5b). Although, it should be noted that the R-phase was not reported to exist in the Al–Mn–Fe (or Co, or Ni) systems [15b]. According to the structural model of the R-phase [27], there are 156 atoms in the unit cell occupying 4-fold, 8-fold and 16-fold sites and its calculated composition is $Al_{124}Mn_{24}TM_8$ [3]. Nevertheless, the R-phase usually forms at lower-Mn and/or higher-Al concentrations than the T-phase. Therefore, it has a tendency for precipitation in the Al-rich T-phase matrix, as documented in the Al–Mn–Pd system [9] and revealed in the Al-Mn-Pt system in the present study. The results of a preliminary study of relevant Al–Mn–Pt alloys, annealed at 700 °C, are in favor of the stability of the Al–Mn–Pt R-phase at this temperature in a compositional region comparable to that of the Al–Mn–Pd system.

4. Conclusions

The previously reported Al–Mn–Pt X-phase was assigned to be a ternary extension of the Al–Mn T-phase. The $Al_{124}Mn_{32}$ stoichiometry of the binary T-phase was argued. Careful analysis of the structure solution and comparison with HAADF images allowed concluding the non-centrosymmetric space group rather than centrosymmetric one, which was commonly associated with the symmetry of the binary T-phase structure. The crystal structure of the $Al_{78}Mn_{17.5}Pt_{4.5}$ T-phase is orthorhombic ($Pna2_1$, a = 14.720(4) Å, b = 12.628(2) Å, c = 12.545(3) Å). A partial atomic model containing 8 Pt, 24 Mn and 36 (out of the expected 124) Al atoms was derived using electron diffraction tomography. Heavy atom positions were compared and found to be in reasonable agreement with proposed earlier non-centrosymmetric model of the binary T phase [5], disputed in [6]. Nanometric plate-like R-phase was found to precipitate in the ternary T-phase grains interior with specific $[001]_T||[001]_R$; $(100)_T||(1\bar{1}0)_R$ orientation relationship. The geometry of the Al–Mn–Pt T-phase region was updated and compared to the equivalent regions in other Al–Mn–TM systems (TM = Cr, Fe, Co, Ni, Cu, Pd).

Acknowledgements

The authors would like to acknowledge Dr. V. Ezersky for assistance with HRTEM and C. Thomas for alloy preparation.

References

1. B. Grushko, A study of the Al–Mn–Pt alloy system, J. Alloys Comp. 792 (2019) 1223-1229. https://doi.org/10.1016/j.jallcom.2019.04.130

[3] Although in Ref. [27] an Al–Mn–Ni R-phase was claimed, this was probably an Al–Mn–Cu phase (see Ref. [**15b**]).

2. M. A. Taylor, The space group of $MnAl_3$, Acta Cryst. 14(1) (1961) 84. https://doi.org/10.1107/S0365110X61000346
3. M. Audier, M. Durand-Charre, M. de Boissieu, AlPdMn phase diagram in the region of quasicrystalline phases, Phil. Mag. B 68(5) (1993) 607-618. https://doi.org/10.1080/13642819308220146
4. K. Hiraga, M. Kaneko, Y. Matsuo, S. Hashimoto, The structure of Al_3Mn: Close relationship to decagonal quasicrystals, Phil. Mag. B 67(2) (1993) 193-205. https://doi.org/10.1080/13642819308207867
5. N. C. Shi, X. Z. Li, Z. S. Ma, K. H. Kuo, Crystalline phases related to a decagonal quasicrystal. I. A single-crystal X-ray diffraction study of the orthorhombic Al_3Mn phase, Acta Cryst. B 50(1) (1994) 22-30. https://doi.org/10.1107/S0108768193008729
6. V. V. Pavlyuk, T. I. Yanson, O. I. Bodak, R. Černý, R. E. Gladyshevskii, K. Yvon, J. Stepien-Damm, Structure refinement of orthorhombic $MnAl_3$. Acta Cryst. C 51(5) (1995) 792-794. https://doi.org/10.1107/S0108270194012965
7. Y. Matsuo, K. Yamamoto, Y. Iko, Structure of a new orthorhombic crystalline phase in the Al-Cr-Pd alloy system, Phil. Mag. Let. 75(3) (1997) 137-142. https://doi.org/10.1080/095008397179688
8. Y. Matsuo, M. Kaneko, T. Yamanoi, N. Kaji, K. Sugiyama, K. Hiraga, The structure of an Al_3Mn-type Al_3(Mn, Pd) crystal studied by single-crystal X-ray diffraction analysis, Phil. Mag. Let. 76(5) (1997) 357-362. https://doi.org/10.1080/095008397178968
9. H. Klein, M. Boudard, M. Audier, M. de Boissieu, H. Vincent, L. Beraha, M. Duneau, The T-Al_3(Mn, Pd) quasicrystalline approximant: chemical order and phason defects, Phil. Mag. Let. 75(4) (1997) 197-208. https://doi.org/10.1080/095008397179624
10. J. Rodrigues-Carvajal, Program FULLPROF-98, Version 0.2, 1998.
11. L. Palatinus, PETS: Program for Analysis of Electron Diffraction Data, Institute of Physics of the Czech Academy of Sciences, (2011).
12. M. C. Burla, R. Caliandro, M. Camalli, B. Carrozzini, G.L. Cascarano, L. De Caro, R. Spagna, IL MILIONE: a suite of computer programs for crystal structure solution of proteins, J. Appl. Cryst. 40(3) (2007) 609-613. https://doi.org/10.1107/S0021889807010941
13. G.M. Sheldrick, SHELXL-97, Program for Crystal Structure Refinement, University of Goettingen, Germany, 1997, release 97-2.
14. B. Grushko, S. Balanetskyy, A study of phase equilibria in the Al-rich part of the Al-Mn alloy system, Inter. J. Mat. Res. 99(12) (2008) 1319-1323, https://doi.org/10.3139/146.101768
15. a) B. Grushko, T. Velikanova, Formation of quasiperiodic and related periodic intermetallics in alloy systems of aluminum with transition metals, Calphad 31(2) (2007), 217-232. https://doi.org/10.1016/j.calphad.2006.12.002.
    b) B. Grushko, D. Pavlyuchkov, S.B. Mi, S. Balanetskyy, Ternary phases forming adjacent to Al_3Mn-Al_4Mn in Al-Mn-TM (TM = Fe, Co, Ni, Cu, Zn, Pd), J. Alloys Comp. 677 (2016) 148-162. https://doi.org/10.1016/j.jallcom.2016.03.220
16. S. Balanetskyy, G. Meisterernst, M. Heggen, M. Feuerbacher, Reinvestigation of the Al–Mn–Pd alloy system in the vicinity of the T- and R-phases, Intermetallics 16(1) (2008) 71-87. https://doi.org/10.1016/j.intermet.2007.08.002
17. B. Grushko, S.B. Mi, Al-rich region of Al–Cu–Mn, J. Alloys Comp. 688 (2016) 957-963. https://doi.org/10.1016/j.jallcom.2016.07.075

18. S. Balanetskyy, G. Meisterernst, M. Feuerbacher, The Al-rich region of the Al–Mn–Ni alloy system. Part I: Ternary phases at 750–950 C, J. Alloys Comp. 509(9) (2011) 3787-3794. https://doi.org/10.1016/j.jallcom.2010.10.185
19. S. Balanetskyy, G. Meisterernst, B. Grushko, M. Feuerbacher, The Al-rich region of the Al–Mn–Ni alloy system. Part II. Phase equilibria at 620–1000 °C, J. Alloys Comp. 509(9) (2011) 3795-3805. https://doi.org/10.1016/j.jallcom.2010.10.114
20. S. Balanetskyy, D. Pavlyuchkov, T. Velikanova, B. Grushko, The Al-rich region of the Al–Fe–Mn alloy system, J. Alloys Comp. 619 (2015) 211-220. https://doi.org/10.1016/j.jallcom.2014.08.232
21. B. Grushko, W. Kowalski, D. Pavlyuchkov, S. Balanetskyy, M. Surowiec, On the constitution of the Al-rich part of the Al–Cr–Mn system, J. Alloys Comp. 468 (2009) 87-95. https://doi.org/10.1016/j.jallcom.2007.12.069.
22. W. Kowalski, B. Grushko, D. Pavlyuchkov, M. Surowiec, A contribution to the Al–Pd–Cr phase diagram, J. Alloys Comp. 496(1-2) (2010) 129-134. https://doi.org/10.1016/j.jallcom.2010.02.033
23. X. Z. Li, K. H. Kuo, The structural model of Al-Mn decagonal quasicrystal based on a new AI-Mn approximant, Phil. Mag. B, 65(3) (1992) 525. https://doi.org/10.1080/13642819208207647
24. U. Kolb, T. Gorelik, M. T. Otten, Towards automated diffraction tomography. Part II—Cell parameter determination, Ultramicroscopy, 108(8) (2008) 763-772. https://doi.org/10.1016/j.ultramic.2007.12.002
25. E.S. Tasci, G. de la Flor, D. Orobengoa, C. Capillas, J.M. Perez-Mato, M.I. Aroyo, An introduction to the tools hosted in the Bilbao Crystallographic Server, EPJ Web Conf. 22 (2012) 9. https://doi.org/10.1051/epjconf/20122200009
26. G. Bergerhoff, M. Berndt, K. Brandenburg, T. Degen, Concerning inorganic crystal structure types, Acta Cryst. B. 55 (1999) 147-156. https://doi.org/10.1107/S0108768198010969
27. K. Robinson, The determination of the crystal structure of $Ni_4Mn_{11}Al_{60}$, Acta Cryst. 7 (1954) 494-497. https://doi.org/10.1107/S0365110X54001570.